Quenching Mechanisms in Bichromophoric, 3_{10}-Helical Aib-Based Peptides, Modulated by Chain-Length-Dependent Topologies

B. Pispisa,*,† L. Stella,† M. Venanzi,† A. Palleschi,‡ C. Viappiani,§ A. Polese,|| F. Formaggio,|| and C. Toniolo||

Dipartimento di Scienze e Tecnologie Chimiche, Universitá di Roma Tor Vergata, 00133 Roma, Italy; Dipartimento di Chimica, Universitá di Roma La Sapienza, 00185 Roma, Italy; Dipartimento di Fisica e INFM, Universitá di Parma, 43100 Parma, Italy; Centro di Studio sui Biopolimeri, CNR; Dipartimento di Chimica Organica, Universitá di Padova, 35131 Padova, Italy

Received September 9, 1999; Revised Manuscript Received November 29, 1999

ABSTRACT: The photophysical and structural features of a series of linear, Aib-based peptides were investigated in methanol solution. These compounds have the general formula P(Aib)$_n$N, where Aib is α-aminoisobutyric acid, N naphthalene, and P the monomethylated protoporphyrin IX, the two latter molecules being covalently attached to the peptide N- and C-termini, respectively, while n = 3, 6, 9, 12, and 15. According to IR and ^{1}H NMR, in all cases the backbone chain populates a 3_{10}-helical structure. Both steady-state and time-resolved fluorescence measurements show a strong quenching of the N emission, whose efficiency depends on the chain length. A corresponding increase of the P fluorescence intensity was also observed, suggesting the occurrence of long-range energy transfer from singlet N* to P, though the N emission quenching parallels the enhancement of P fluorescence intensity in the short compounds only, i.e., for n = 3, 6, and 9. In the longer peptides (n = 12 and 15) a competitive quenching mechanism, possibly an electron-transfer process from P ground-state to ^{1}N*, is likely to occur. Transient absorption spectra of P(Aib)$_6$N and P(Aib)$_{15}$N in aereated methanol solution show marked differences between the two peptides, suggesting different deexcitation pathways. Molecular mechanics calculations show differences in the topology as the chain length of the peptides increases, which are thought to be primarily responsible for the singlet energy transfer vs electron-transfer competition.

Introduction

Photoexcitation of an electron donor−S−acceptor (d−S−a) system, where S is a spacer, leads to exciplex formation, singlet excitation energy transfer, or electron transfer, depending on a number of factors, e.g., the nature of both donor and acceptor, the intervening medium (solvent or spacer), temperature, etc.[1] For instance, long-range energy transfer occurs when the emission spectrum of the donor overlaps the absorption spectrum of the acceptor and when the emission and absorption dipoles of the donor and acceptor molecules are at a certain distance and properly oriented.[2] On the other hand, exciplex formation and electron transfer are thought to occur via charge-transfer complexes,[3] but it is still unknown which type of encounter complex favors one or the other process. Indeed, irrespective of the model used to describe the electron-transfer (ET) process, a requirement for efficient ET is that the reacting species be appropriately coupled vibronically in the transition state.[4,5] The kind of bridge and the structural features of the assembly thus play a critical role in facilitating ET, as recently shown, e.g., by Isied and coworkers.[6] By an increase in the chain length of the proline spacer between Ru(II) and Co(III) complex ions,[6a] the peptide attains a helical structure that facilitates electron transfer from Ru(II) to Co(III), as compared to the disordered peptide. This was attributed to a better orbital matching in the donor-to-bridge (d−S) and bridge-to-acceptor (S−a) matrix elements,[4b] controlling the coupling pathway between the reacting pair. Electronic structure calculations show that electronic coupling varies considerably with system conformation, even when the effective d/a separation remains practically constant.[5b] For instance, Bolton and coworkers[7a] have shown that, despite the edge-to-edge distance between the donor (tetraarylporphine) and the acceptor (*p*-benzoquinone) remaining practically constant on going from bicyclooctane to cyclobutane bridge, the ET rate in methylene chloride increases by almost 2 orders of magnitude. This is probably because the cyclobutane bridge orients the d/a pair more favorably than the other spacer.

To address the problem of the structure of d−S−a systems in solution undergoing photoexcited transfer processes, we started investigating the photophysics of naphthalene (N) and monomethylated protoporphyrin IX (P), covalently bound to ε-amino groups of poly(L-lysine).[8] On going from pH 7 to 11, i.e., from the disordered to the ordered polymeric matrix, quenching of excited naphthyl chromophores was found to chiefly occur by two competitive processes. One was interconversion to the triplet state, taking place when the sample was randomly coiled, and the other was intramolecular electron transfer from ground-state porphyrin, when the polypeptide was in the α-helical conformation. Interestingly, molecular mechanics calculations showed that in alkaline solution the aromatic moieties were lying on the surface of the ordered chain, in an edge-to-edge geometry, despite the degrees of conformational freedom of the chromophores linkages.[9]

More recently, we studied the photophysical behavior in methanol or water/methanol solution of short (6−10 residues), Ala-based peptides, carrying the same P and N chromophores covalently bound to the ε-amino groups of L-Lys residues. In all cases the backbone chain was

† Universitá di Roma Tor Vergata.
‡ Universitá di Roma La Sapienza.
§ Universitá di Parma.
|| Universitá di Padova.

10.1021/ma991539o CCC: $19.00
Published on Web 01/15/2000

Chart 1

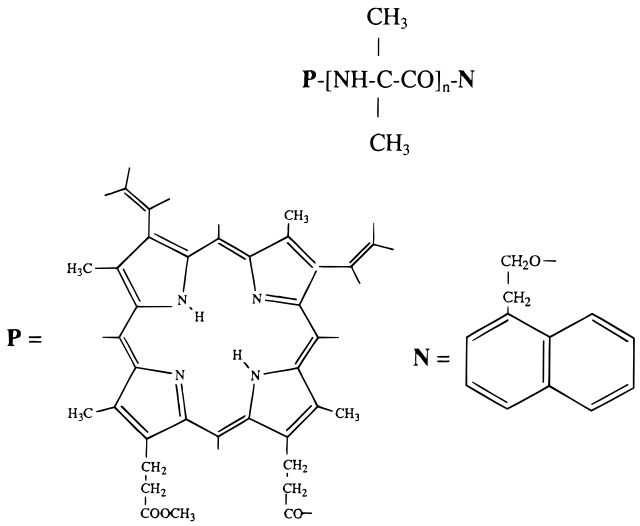

found to populate an α-helical structure, but, unexpectedly, quenching of N chromophore occurred by intramolecular N* → P transfer of excitation energy.[10] This result is probably related to the observation that the two chromophores in the ordered peptides attain a stacked, almost face-to-face geometry, the backbone chains being too short to accommodate the donor−acceptor pair in an edge-to-edge fashion. The same effect was found in linear, Aib-based peptides populating a 3_{10}-helical conformation.[11]

To gain more insight into the relationship between the mechanism of quenching in the N*−P pair and structural features of the peptide matrix, we have been studying the photophysics of a series of Aib-based peptides of different chain lengths, i.e., P(Aib)$_n$N, where n = 3, 6, 9, 12, and 15, as illustrated in Chart 1. By assuming that the backbone chain attains a 3_{10}-helical conformation, owing to the proven ability of Aib to form 3_{10}-helices[12] because of the steric constraints of the *gem*-dimethyl group, the values of n in the spacer were chosen so as the chromophores would lie on the same side of the helix, from one to five turns apart.

Both the rigidity of the 3_{10}-helix and the very short linkages of the probes, which are directly bound to the backbone chain, are expected to give rise to rather compact structures. This would be reflected in a narrow distribution of conformers, even for the longer terms of the series. In addition, because of the relatively large range of lengths of the spacer, one would also expect the occurrence of different topologies in the d−S−a systems investigated, which may bring about different quenching mechanisms of N*.

Experimental Section

Materials. Protoporphyrin IX monomethylation was achieved by a solid-phase method,[13] by anchoring the porphyrin molecule to a low-degree substituted Wang resin (Novabiochem, Läufelfingen, Switzerland), followed by monomethylation and final deblocking from the resin. We were unable to separate the two resulting 2- and 18-monoesters (positional isomers), despite a number of HPLC attempts, under different experimental conditions.

Peptide synthesis was performed in solution from the C-terminal residue using benzyloxycarbonyl (Z) as the N-terminal protecting group. Z−Aib$_3$−O*t*Bu[14] (O*t*Bu is *tert*-butoxy) was first synthesized by reaction of the symmetrical anhydride (Z−Aib)$_2$O[15] with H−Aib$_2$−O*t*Bu, the latter being in turn obtained from the corresponding Z-protected peptide by catalytic hydrogenation. The N$^\alpha$-protected tripeptide free acid,[14] obtained by treatment of the corresponding *tert*-butyl ester with trifluoroacetic acid (TFA), was converted into the corresponding 5-(4*H*)-oxazolone by reaction with 1 equiv of *N*-ethyl-*N*′-(3-dimethylaminopropyl)carbodiimide (EDC) and subsequently allowed to react with 1-naphthyl-2-ethanol [HOCH$_2$−CH$_2$−(1)-Naph] in the presence of a catalytic amount of 4-(dimethylamino)pyridine (DMAP), affording Z−Aib$_3$−OCH$_2$−CH$_2$−(1)-Naph (method 1). The higher homologues Z−Aib$_n$−OCH$_2$−CH$_2$−(1)-Naph (n = 6, 9, 12, 15) were obtained by fragment condensation, by activating the carboxylic group of the N$^\alpha$-protected tri- or hexapeptides via oxazol-5(*4H*)-one[16] (method 2). The N$^\alpha$-functionalization of the monomethylated protoporphyrin IX (P) peptides was obtained by reaction of P, activated at the free carboxylic group by the EDC/1-hydroxy-7-aza-benzotriazole (HOAt)[17] method, with H−Aib$_n$−OCH$_2$−CH$_2$−(1)-Naph (n = 3, 6, 9, 12, 15) (method 3).

Typical coupling procedures were the following.

P. (i) Linkage to the Resin. To a stirred solution of P (0.406 g, 0.72 mmol) in *N*,*N*′-dimethylformamide (DMF) (4 mL) at 0 °C was added EDC (0.338 g, 1.76 mmol). After a few minutes, the solution was poured in a round-bottom flask containing the *p*-benzyloxybenzyl alcohol Wang resin[18] (1.218 g), previously swelled in DMF. DMAP (0.101 g, 0.82 mmol) was added and the reaction mixture was allowed to react overnight.

(ii) P-Resin. To the P-resin suspension EDC (0.179 g, 0.93 mmol) were added DMAP (0.050 g, 0.36 mmol) and methanol (MeOH) (3 mL). After the reaction mixture was stirred for 24 h, the resin was filtered, washed with DMF, CH_2Cl_2, and Et_2O, and finally dried over P_2O_5. **(iii) P.** The P-resin (1.45 g) was dissolved in 10 mL of a 1:1 CH_2Cl_2−TFA solution. The reaction mixture was allowed to stir for 60 min. The resin was filtered off, and the product was purified by flash-chromatography on a silica gel column and eluted with a 98:2 $CHCl_3$−EtOH solvent mixture. Crystallization from EtOH afforded the product in 31% yield.

Z−Aib$_3$−OCH$_2$−CH$_2$−(1)-Naph [Z−(Aib)$_3$N] (Method 1). To a stirred solution of the 5-(4*H*)-oxazolone from Z−Aib$_3$−OH[19] (1.36 g, 3.51 mmol) and HOCH$_2$−CH$_2$−(1)-Naph (0.77 g, 4.48 mmol) in 10 mL of anhydrous acetonitrile (MeCN) was added DMAP (0.225 g, 1.84 mmol). The reaction mixture was refluxed for 24 h, and the solvent was removed under reduced pressure. The peptide was purified by flash chromatography on a silica gel column and eluted with a 98:2 $CHCl_3$:EtOH solvent mixture. Crystallization from ethyl acetate (EtOAc)/petroleum ether (PE) afforded the product in a 83% yield.

Z−Aib$_9$−OCH$_2$−CH$_2$−(1)-Naph [Z−(Aib)$_9$N] (Method 2). To a stirred solution of the 5-(4*H*)-oxazolone from Z−Aib$_3$−OH[19] (0.24 g, 0.63 mmol) in 5 mL of anhydrous MeCN was added H−Aib$_6$−OCH$_2$−CH$_2$−(1)-Naph (0.62 mmol) [obtained from a Pd-catalyzed hydrogenation in MeOH of the corresponding Z−hexapeptide ester (0.51 g, 0.62 mmol)]. The reaction mixture was refluxed for 7 h. The resulting precipitate was filtered, washed with Et_2O, and dried. Crystallization from MeCN/Et_2O afforded the product in a 54% yield.

P−Aib$_3$−OCH$_2$−CH$_2$−(1)-Naph [P(Aib)$_3$N] (Method 3). To a stirred solution of P (0.0297 g, 0.052 mmol) and HOAt (0.0108 g, 0.079 mmol) in 2 mL of anhydrous CH_2Cl_2 at 0 °C was added EDC·HCl (0.0168 g, 0.087 mmol). Then, H−Aib$_3$−OCH$_2$−CH$_2$−(1)-Naph (0.0254 g, 0.060 mmol) [obtained from a Pd-catalyzed hydrogenation in MeOH of the corresponding Z−tripeptide ester (0.060 mmol)], dissolved in 1 mL of anhydrous CH_2Cl_2, was added, followed by *N*-methylmorpholine (NMM) (5.8 λ, 0.052 mmol). The reaction mixture was allowed to stir at room temperature for 2 days. The solvent was removed under reduced pressure, and the peptide was purified by flash chromatography on a silica gel column and eluted with a 97:3 $CHCl_3$−EtOH solvent mixture. Crystallization from $CHCl_3$/PE afforded the product in a 61% yield.

The physical and analytical properties of the peptides are listed in Table 1. Melting points were determined by a Leitz (Wetzlar, Germany) model Laborlux 12 apparatus and are not corrected. Thin-layer chromatography (TLC) was performed on Merck (Darmstadt, Germany) Kieselgel 60F$_{254}$ precoated

Table 1. Physical Properties of Peptides and Intermediates

compound	mp (°C)	recryst solvent [a]	TLC[b] R_{F1}	R_{F2}	R_{F3}	mass $(M+H)^+$ $(M+Na)^+$	IR[c]
Z−Aib_3−OCH_2−CH_2−(1)-Naph	123−125	EtOAc/PE	0.85	0.95	0.40		3377, 3322, 1724, 1697, 1681, 1651, 1597
Z−Aib_6−OCH_2−CH_2−(1)-Naph	183−185	EtOAc/PE	0.65	0.95	0.35		3325, 1733, 1702, 1662, 1528
Z−Aib_9−OCH_2−CH_2−(1)-Naph	213−215	MeCN	0.70	0.95	0.30	1097	3313, 1734, 1658, 1529
Z−Aib_{12}−OCH_2−CH_2−(1)-Naph	238−240	MeCN	0.75	0.95	0.30	1350	3298, 1720, 1656, 1532
Z−Aib_{15}−OCH_2−CH_2−(1)-Naph	296−298	MeCN	0.75	0.95	0.20	1605	3297, 1702, 1656, 1534
Prot-IX−OMe−Aib_3−OCH_2−CH_2−(1)-Naph	170−172	$CHCl_3$/PE	0.85	0.95	0.45	988 1011	3312, 1731, 1657, 1527
Prot-IX−OMe−Aib_6−OCH_2−CH_2−(1)-Naph	220−222	EtOAc/ PE	0.70	0.95	0.40	1243 1265	3430, 3312, 1733, 1657, 1526
Prot-IX−OMe−Aib_9−OCH_2−CH_2−(1)-Naph	162−164	EtOAc/PE	0.95	0.95	0.35	1497 1520	3309, 1734, 1656, 1531
Prot-IX−OMe−Aib_{12}−OCH_2−CH_2−(1)-Naph	260−262	MeOH	0.95	0.95	0.35	1753 1776	3307, 1734, 1657, 1531
Prot-IX−OMe−Aib_{15}−OCH_2−CH_2−(1)-Naph	> 300	$CHCl_3$/MeOH	0.95	0.95	0.35	2009 2031	3293, 1733, 1655, 1533

[a] Key: EtOAc, ethyl acetate; PE, petroleum ether; MeCN, acetonitrile; MeOH, methanol. [b] The three R_f values refer to different solvent mixtures (see Experimental Section). [c] The solid-state IR absorption spectra were obtained in KBr pellets (only bands in the 3450−3300 cm^{-1} and 1850−1500 cm^{-1} regions are reported).

plates using the following solvent systems: 1, $CHCl_3$−EtO, 9:1; 2, Bu^nOH−AcOH−H_2O, 3:1:1, where Bu^nOH is *n*-butanol and AcOH acetic acid; 3, toluene−EtOH, 7:1. The chromatograms were examined by ultraviolet fluorescence or developed by chlorine−starch−potassium iodide or ninhydrin chromatic reaction, as appropriate. All compounds were obtained in a chromatographically homogeneous state.

Spectrograde deuteriochloroform (99.8% *d*) was purchased from Fluka (Buchs, Switzerland) and spectrograde methanol from C. Erba (Milan, Italy).

Methods. Mass spectra were recorded by a *time-of-flight* Reflex mass spectrometer using the MALDI ionization technique.

IR spectra, monitored for peptide characterization, were obtained in KBr pellets on a Perkin-Elmer 580B spectrophotometer, equipped with a Perkin-Elmer 3600 IR data station. FT-IR spectra of the peptides were instead recorded on a Perkin-Elmer 1720 X spectrophotometer, nitrogen flushed and equipped with a sample-shuttle device, at 2 cm^{-1} nominal resolution, averaging 100 scans. Solvent (baseline) spectra were obtained under the same conditions. The path lengths of the cells were 0.1, 1.0, and 10 mm (CaF_2 windows).

The ^1H NMR spectra, monitored for peptide characterization, were recorded on a Bruker AC 200 or AC 250 spectrometer, while NMR titrations and 2D-NMR experiments were performed using a Bruker AM 400 spectrometer. Data collected from bidimensional experiments were processed by a Bruker X-32 elaborator using a UXNMR program. Measurements were carried out in deuteriochloroform (99.96% *d*; Acros, Geel, Belgium) and deuterated dimethyl sulfoxide (DMSO) (99.96% d_6, Acros).

Steady-state fluorescence spectra were recorded on a SPEX Fluoromax spectrofluorometer, operating in SPC mode. Quantum yields were obtained by using naphthalene in cyclohexane as reference: $\Phi_N = 0.23 \pm 0.01$.[20] Nanosecond decays were measured by a CD900, SPC lifetime apparatus from Edinburgh Instruments. Excitation in the UV region was achieved by an arc flashlamp filled by ultrapure hydrogen (300 mmHg; fwhm = 1.2 ns at 30 kHz repetition rate). The decay curves were fitted by a nonlinear least-squares analysis to exponential functions through an iterative deconvolution method. All solutions were bubbled for 20 min with ultrapure argon before each measurement.

The laser flash photolysis setup was based on a XeCl excimer laser (Lambda Physik, EMG 50, $\lambda = 308$ nm, pulse width = 8 ns). The beam was attenuated by means of neutral density filters and passed through a square (1 cm) fused silica fluorescence cuvette. Part of the beam is split to an energy meter (Laser Precision RJ-7620) equipped with a pyroelectric energy probe (Laser Precision RJp-735) to monitor fluctuations in the energy of the laser pulses. Detection of transient absorption was performed by a 450 W high-pressure Xe lamp which was focused into the cuvette after filtering off the ultraviolet portion of the spectrum by a low-pass filter (cutoff wavelength at 350 nm). The beam was then focused into a monochromator (Jobin-Yvon H25) and the monochromatic light was collected with a silicon avalanche photodiode (Hamamatsu,S2385). The signal was then amplified and digitized by a digital oscilloscope (Lecroy 9370, 1GHz, 1Gs/s). The setup allowed monitoring of transient absorption between 400 and 900 nm with laser-limited time resolution. All experiments were carried out at room temperature.

Other apparatuses were already described.[10,11]

Results and Discussion

UV−Vis, IR, and ^1H NMR Spectra. UV−vis absorption measurements in methanol exhibit the well-known transitions of N ($\epsilon_{224} = 66\,000$, $\epsilon_{283} = 6100$ M^{-1} cm^{-1}) and spectral features of P ($\epsilon_{400} = 125\,000$ M^{-1} cm^{-1}; Q-bands = 503, 538, 575, 629 nm). In all compounds investigated, the absorption spectra overlap the sum spectrum of single P and N chromophores, which rules out ground-state interactions between the chromophores.

IR measurements were carried out in $CDCl_3$ for three different concentrations (0.1, 1, and 10 mM) on the Z−$(Aib)_n$N peptides (n = 3, 6, 9, 12, 15). In the N−H absorption region, two characteristic bands were observed at around 3430 cm^{-1}, associated with the stretching vibration of N−H groups not involved in H-bond interactions, and at around 3330 cm^{-1}, typical of H-bonded N−H groups. As expected, the relative area of this red-shifted transition increases as the length of the backbone chain increases, thereby denoting a greater number of Aib residues participating in the H-bond network.[21a,b,22]

Where the integrated intensities of the bands of H-bonded (A_b) and free (A_f) N−H groups were calculated, the ratio A_b/A_f was found to linearly depend on the number of Aib residues in the backbone chain, as shown in Figure 1. The intercept of the straight line for $(A_b/A_f) = 0$, which corresponds to the number of residues in the backbone chain that are one unit too short for a helical turn formation by an intramolecular hydrogen bond, is $n \approx 2$. This figure, which is that predictable for

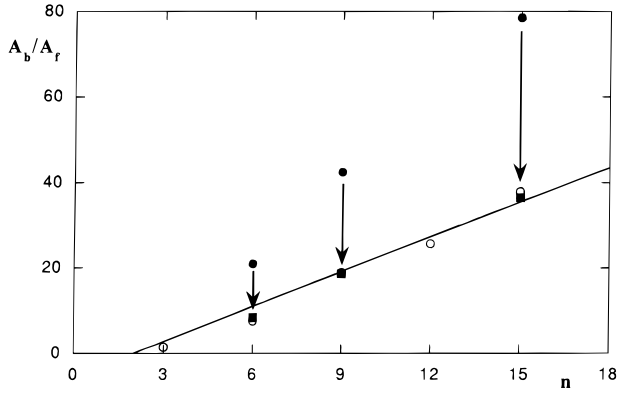

Figure 1. Plot of A_b/A_f ratio against the number of Aib residues in the spacer, *n*, for the Z−(Aib)$_n$N and P(Aib)$_n$N peptides. The intercept at $A_b/A_f = 0$ corresponds to the number of peptide groups in the backbone chain that are one unit too short for a helical turn formation by an intramolecular H-bond. Key: open symbols, Z−(Aib)$_n$N; full symbols, P(Aib)$_6$N, P(Aib)$_9$N and P(Aib)$_{15}$N. The arrows show the shift of the A_b/A_f values, once correction for the additional intramolecular H-bond in the latter peptides is made.[23] Concentrations: 0.1−1 mM, in $CDCl_3$.

Chart 2. Schematic Representation of a 3_{10}-Helical Section in Cylindrical Coordinates of (Aib)$_n$ with Distances in Å

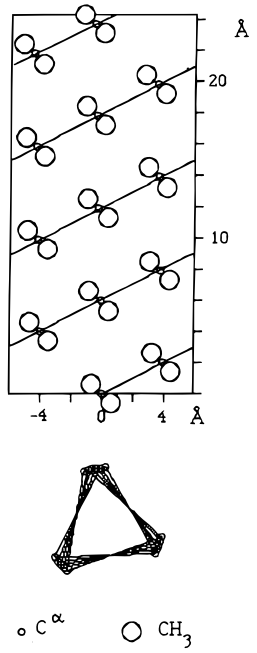

an H-bonding scheme of the $i \rightarrow i + 3$ (C_{10}) type, strongly suggests that Z−(Aib)$_n$N attain a 3_{10}-helix structure. The geometric features of an (Aib)$_n$ 3_{10}-helix are schematically illustrated in Chart 2. Consistently, analysis of the C═O stretching region reveals an amide−I mode at 1663−1657 cm^{-1}, typical of helical conformations.[21c]

The same spectral features were observed when IR measurements were carried out on P(Aib)$_n$N, but higher values of the A_b/A_f ratio were observed (Figure 1). This is suggestive of additional intramolecular H-bond interactions between the C═O ester porphyrin group and a N−H group in the backbone chain. Once these interactions were properly accounted for,[23] the values of the A_b/A_f ratio of P(Aib)$_n$N nicely fall on the straight line of the Z-analogues, indicating that the 3_{10}-helical structure is conserved, as already observed for other linear, Aib-based peptides in methanol or water/methanol solution.[11]

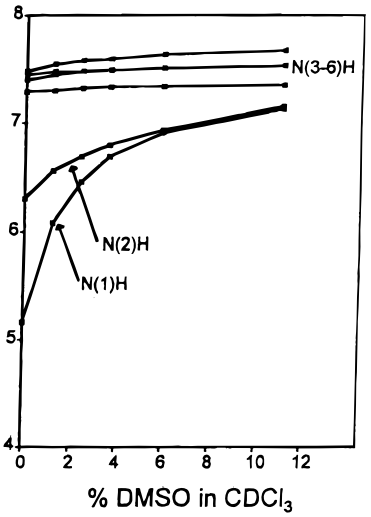

Figure 2. Typical ^{1}H NMR titration of N−H protons of Z−(Aib)$_6$N in $CDCl_3$ by DMSO. The chemical shifts of N(1)−H and N(2)−H protons are significantly sensitive to the addition of DMSO, while those of N(3−6)−H protons are not, displaying a behavior typical of buried protons (see text).

We next investigated the ^{1}H NMR spectra of the Z−(Aib)$_n$N derivatives in $CDCl_3$. This because the Z-analogues allow us to analyze the N−H backbone signals within the region of 7−8 ppm without the disturbing overlap of the absorptions of the protoporphyrin vinyl protons. Compared to P systems, the Z-aromatic protons give rise to a sharp, easier to identify, multiplet. The presence of the Z group also favors the unequivocal assignment of the N-terminal urethane proton, which resonates at higher fields than the corresponding amide protons.

Titration of N−H protons by the hydrogen-bonding acceptor solvent DMSO[24] reveals that only two of the N−H absorptions were perturbed, as shown in Figure 2 for a typical Z−peptide (hexapeptide). If the N−H groups were numbered in the conventional way, namely starting from the N− terminus of the backbone chain, two classes of protons could be observed. Class i [N(1)−H and N(2)−H protons] includes protons whose chemical shifts are significantly sensitive to the addition of DMSO, while class ii [from N(3)−H to N(6)−H protons] includes those displaying a behavior characteristic of buried protons. All NH proton resonances were assigned by means of 2D ROESY experiments. Similar results were obtained for the other homopeptides.

These findings are in full agreement with a previous systematic study performed by some of us on a series of Aib−homopeptide *tert*-butyl esters,[25] and strongly suggests that the most populated structure adopted in $CDCl_3$ solution by the N$^\alpha$-terminal protected or blocked Aib homopeptide naphthyl esters is the 3_{10}-helix, as already observed by the IR spectra.

Steady-State Fluorescence. Typical steady-state fluorescence spectra of N* in methanol are illustrated in Figure 3. A substantial quenching of N singlet emission by the bound protoporphyrin molecule can be noted. The efficiency of the quenching process, E_N, as given by $[1 - (\Phi_{PN}/\Phi_N)]$, where Φ_{PN} is the quantum yield of N* in P(Aib)$_n$N, are reported in Table 2. The quantum yield of N* in Z−(Aib)$_n$N (reference), Φ_N, is similar to that of free naphthalene, indicating that naphthyl−peptide interactions are very weak.

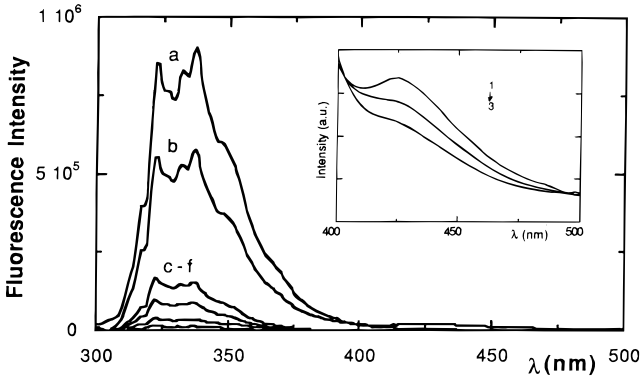

Figure 3. Steady-state fluorescence spectra of P(Aib)$_n$N and the reference sample Z−(Aib)$_3$N (curve a) in methanol. Key: curve b, P(Aib)$_{15}$N; curve c, P(Aib)$_{12}$N; curve d, P(Aib)$_9$N; curve e, P(Aib)$_6$N; curve f, P(Aib)$_3$N. Insert: spectra of P(Aib)$_{15}$N in the 400−500 nm wavelength region, in solvents of different polarity (1, methanol; 2, ethanol; 3, dioxane). The solvent-dependent shoulder at around 420 nm is thus assigned to an emissive charge recombination process.

Table 2. Steady-State Efficiencies of P(Aib)$_n$N in Methanol

peptides	E_N[a]	E_P[b]
P(Aib)$_3$N	0.99	1.00
P(Aib)$_6$N	0.96	1.00
P(Aib)$_9$N	0.90	1.00
P(Aib)$_{12}$N	0.84	0.40
P(Aib)$_{15}$N	0.40	0.19

[a] $\lambda_{ex} = 280$, $\lambda_{em} = 340$ nm; $E_N = 1 - (\Phi_{PN}/\Phi_N)$, where Φ_{PN} is the quantum yield of N* in P(Aib)$_n$N and Φ_N (≈ 0.22) that in (Aib)$_n$N. [b] $\lambda_{ex} = 280$, $\lambda_{em} = 630$ nm; $E_P = [(I_{PN}/I_P) - 1](\epsilon_P C_P/\epsilon_N C_N)$, where $I_P = \epsilon_P C_P \Phi_P$ and $I_{PN} = \epsilon_P C_P \Phi_P + \epsilon_N C_N \Phi_P E_P$ are the fluorescence intensities of protoporphyrin in (Aib)$_n$P and in P(Aib)$_n$N, respectively, while C_P and C_N are the concentrations of the acceptor and donor chromophores. In all cases, the uncertainty is better than 6%.

Upon inspection of Table 2, it appears that the quenching efficiency E_N depends on the chain length, i.e., on the value of n, and parallels with the efficiency of the fluorescence rise in P, E_P, in the shorter compounds ($n = 3, 6, 9$). This indicates that the energy lost in the deactivation of the excited naphthyl chromophore is completely transferred to the porphyryl group, within experimental error, which, in turn, implies that a N* → P energy transfer process does occur in these compounds. This is further confirmed by the results of the differential excitation spectra, reported in Figure 4. They are performed by exciting the spectral region of the naphthalene absorption (240−300 nm), fixing the wavelength at the porphyrin emission ($\lambda_{em} = 630$ nm), and subtracting the spectrum of porphyrin from those of P(Aib)$_n$N. As a result, the typical patterns of naphthalene are observed, thereby implying that the excitation energy of N* is transferred to P.

Finally, two further points are worth noting. First, the E_N and E_P values in Table 2 differ for the longer peptides, namely $n = 12$ and 15, suggesting the occurrence of an additional, competitive quenching mechanism, other than energy transfer; second, the steady-state fluorescence spectrum of P(Aib)$_{15}$N exhibits a rather broad shoulder at $\lambda_{em} \approx 420$ nm, as shown in the insert of Figure 3. Its intensity depends on the polarity of the solvent medium, so that the band can be assigned to a (weakly) emissive charge recombination process between the donor (P) and acceptor (N*).[26]

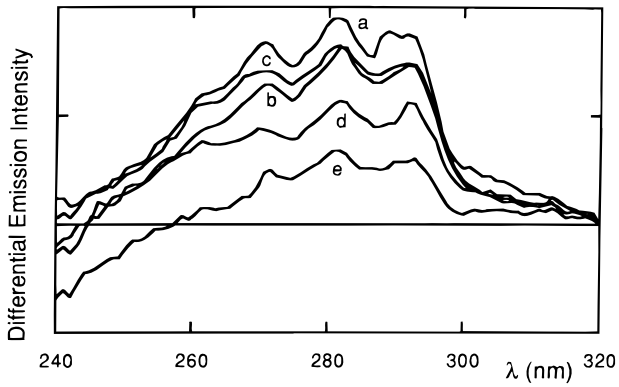

Figure 4. Differential excitation spectra of P(Aib)$_n$N against P, carried out by exciting the spectral region of N absorption (240−300 nm), and fixing the wavelength at the porphyrin emission ($\lambda_{em} = 630$ nm). Key: curve a, P(Aib)$_3$N; curve b, P(Aib)$_6$N; curve c, P(Aib)$_9$N; curve d, P(Aib)$_{12}$N; curve e, P(Aib)$_{15}$N. The typical spectral patterns of naphthalene can be noted.

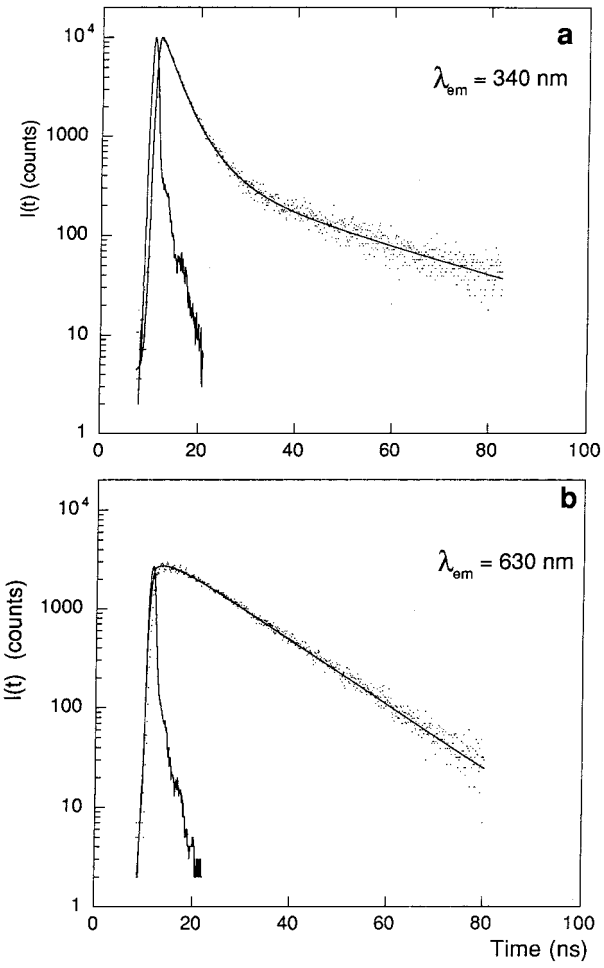

Figure 5. Typical time decay profiles of fluorescence of N* (a: $\lambda_{ex} = 280$, $\lambda_{em} = 337$ nm) and P* (b: $\lambda_{ex} = 280$, $\lambda_{em} = 630$ nm) in methanol. The full lines represent the best fit to the experimental data by a three-exponential (a) and two-exponential (b) decay for P(Aib)$_9$N. The lamp profile is also shown.

Time-Resolved Fluorescence. Typical time decay profiles in methanol of N* ($\lambda_{ex} = 280$, $\lambda_{em} = 337$ nm) and P* ($\lambda_{ex} = 280$, $\lambda_{em} = 630$ nm), are shown in Figure 5. The curves were well fitted by a multiexponential decay, eq 1, where i goes from 1 to 3 for N*, and from 1 to 2 for P*. In contrast, the time decay of the reference

Table 3. Fluorescence Lifetimes of N* in Methanol at 25 °C[a]

peptides	τ_{N1} (ns)	α_{N1}	τ_{N2} (ns)	α_{N2}	τ_{N3} (ns)	α_{N3}	χ^2
$P(Aib)_3N$	0.3	0.93	8.8	0.03	26.8	0.04	1.37
$P(Aib)_6N$	1.0	0.96	6.0	0.03	26.5	0.01	1.43
$P(Aib)_9N$	2.3	0.73	4.8	0.23	26.7	0.04	1.14
$P(Aib)_{12}N$	3.3	0.26	7.4	0.71	24.0	0.03	1.26
$P(Aib)_{15}N$	2.8	0.09	10.1	0.60	23.8	0.31	1.09

[a] $\lambda_{ex} = 280$, $\lambda_{em} = 337$ nm; the time decay of N* in the $(Aib)_nN$ (reference) in methanol is $\tau_{N0} = 28.8 \pm 1.2$ ns. In all cases the lifetime uncertainty is better than 5%, while that of the preexponents is around 20%.

Table 4. Fluorescence Lifetimes of P* in Methanol at 25 °C[a]

peptides	τ_{P1} (ns)	α_{P1}	τ_{P2} (ns)	α_{P2}	χ^2
$P(Aib)_3N$	0.2	−0.012	14.6	0.012	1.11
$P(Aib)_6N$	0.5	−0.010	13.8	0.013	1.09
$P(Aib)_9N$	3.0	−0.004	12.9	0.013	1.27
$P(Aib)_{12}N$	5.7	−0.004	12.9	0.012	1.15
$P(Aib)_{15}N$	20.7	−0.001	15.6	0.009	1.28

[a] $\lambda_{ex} = 280$, $\lambda_{em} = 630$ nm; the time decay of protoporphyrin (reference) in methanol is $\tau_{P0} = 13.4 \pm 0.7$ ns. In all cases the lifetime uncertainty is better than 5%, while that of the preexponents is around 15%.

samples, Z−$(Aib)_n$N or porphyrin alone, was found to be strictly monoexponential, i.e., $\tau_{N0} = 28.8 \pm 1.2$ and $\tau_{P0} = 13.4 \pm 0.7$ ns.

$$I(t) = \sum_i \alpha_{N(P)i} \exp[-t/\tau_{N(P)i}] \qquad (1)$$

Table 3 lists the lifetimes and preexponents of the three-component exponential decay of N*, while Table 4 lists those of the biexponential decay of P*. The lifetimes distribution analysis of the decays (not shown) is in full agreement with the results of the discrete model reported in Table 3, in the sense that it gives narrow distributions, whose centers and relative weights compare well with those shown in the table.

The high purity of the peptides examined makes it reasonable to rule out the presence of contaminants and attribute each decay component listed in Table 3 to one conformer populating the solution. In principle, a single decay time could arise either from a single conformer or from many conformers, all having a very similar quenching rate. However, in the case of Förster energy transfer, the quenching rate is determined by both interprobe distance and orientation.[2,27] Therefore, the latter hypothesis would imply that all conformers corresponding to a given lifetime have also a very similar structure, so that, within the experimental resolution, they can be considered as a single conformer. Indeed, there is another possibility; i.e., different orientations and distances could exactly balance their effects, giving rise to quite the same quenching rates. This possibility is highly unlikely, however, and is ruled out for the good correlation between the calculated and experimental quenching efficiencies, as shown below.

In all cases, the overall quenching efficiencies of steady-state, $E_N = 1 - (\Phi_{PN}/\Phi_N)$, and time-resolved, $E'_N = 1 - (\langle\tau\rangle/\tau_{N0})$, fluorescence, where $\langle\tau\rangle = \sum_i \alpha_{Ni}\tau_{Ni}$ is the average time decay, compare well, within experimental error. This implies that a static quenching process and (strong) ground-state interactions are absent.

As far as the time decays of P* are concerned, the main inference to be drawn from Table 4 is that the τ_{P1} lifetimes have negative preexponents, thus denoting a process populating the S_1 emissive state. They steadily decrease, in absolute value, with increasing interprobe distance, which suggests that the energy transfer process is more and more depleted along the series. In addition, the τ_{P2} lifetimes are nearly constant, being close to that of the protoporphyrin itself. This result indicates that P excited states are not involved in the N* quenching, otherwise one would have observed τ_{P2} values differing from that of the unperturbed protoporphyrin. Therefore, the competitive mechanism put forward to explain the photophysical results in the longer peptides ($n > 9$) could well be an electron-transfer process from the P ground-state to $^1N^*$,[8] as suggested above.

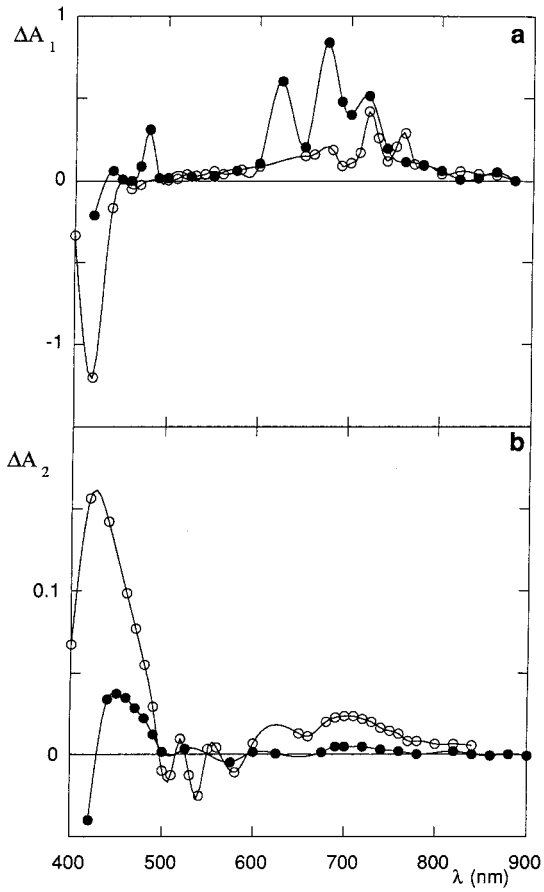

Figure 6. Transient absorption spectra of $P(Aib)_6N$ (empty symbols) and $P(Aib)_{15}N$ (full symbols) in aerated methanol. They are best described by a two-exponential function, with the lifetimes given in the text. The a and b plots refer to each lifetime component.

Flash Photolysis. Transient absorption measurements were carried out on $P(Aib)_6N$ and $P(Aib)_{15}N$ in air saturated methanol solution, leading to absorption signals in the nanosecond domain for both peptides (Figure 6). The fitting of the data was performed by a sum of two exponential decay functions. The first recovered lifetimes are 27 ± 1 for $P(Aib)_6N$ and 11 ± 1 ns for $P(Aib)_{15}N$ (Figure 6a). Note that only the spectrum of the first compound is dominated by the bleaching in the Soret region and that above 450 nm the spectra are positive everywhere, indicating that in both cases the spectrum of the photochemical product comprises bands with high absorbance relative to the ground-state porphyrin.

The spectrum associated with the other lifetimes, which are 216 ± 5 for $P(Aib)_6N$ and 209 ± 5 ns for

$P(Aib)_{15}N$ (Figure 6b), is typical of a T−T absorption in both compounds, as confirmed by the rate constant for oxygen quenching [$k_q = (3.6 \pm 0.1) \times 10^9$ and $(3.9 \pm 0.1) \times 10^9$ $M^{-1}\cdot s^{-1}$],[28] though the much stronger intensity observed in $P(Aib)_6N$ indicates that the triplet state of $P(Aib)_{15}N$ is less populated.

The transient absorption spectrum of $P(Aib)_{15}N$ in Figure 6a exhibits new absorption features, as compared to that of $P(Aib)_6N$, within the wavelength region of 400−500 and 600−800 nm. As already noted, the bleaching in the Soret region of $P(Aib)_{15}N$ is markedly different from that of $P(Aib)_6N$, while, in principle, it should be the same. Since both the extinction coefficient and population of the singlet state are the same for both peptides, while the triplet state does not contribute to the spectrum because it decays much more slowly, according to the foregoing figures, the large difference in the absorptions in the 400−500 nm region can be ascribed to an additional, positive, band in $P(Aib)_{15}N$. Cancellation of this band with that arising from the bleaching of the Soret band gives rise to the small absorption at 480 nm. According to literature data on flash-photolysis studies on functionalized porphyrins, charged porphyrin moieties, i.e., $P^{\bullet+}$, are characterized by a weak band at 478−485 nm.[28,29] The spectra of porphyrin radical cations are very distinctive, in that the absorbing $P^{\bullet+}$ entity has two other characteristic overlapping peaks at 680 and 725 nm.[29a] Since two new overlapping absorptions appear in $P(Aib)_{15}N$, but not in $P(Aib)_6N$, at the same wavelengths, i.e., around 680 and 730 nm, it may be reasonably concluded that a transient porphyrin radical is produced by photoexcitation of $P(Aib)_{15}N$ only. Although further experiments are needed to get a definite confirmation of this idea, the results of Figure 6 are fully consistent with the hypothesis that an additional quenching mechanism of N*, other than a $^1N^* \rightarrow P$ energy transfer, takes place in $P(Aib)_{15}N$, possibly a $P \rightarrow {}^1N^*$ ET process.

Molecular Modeling. Molecular mechanics calculations were performed to gather information on the geometric and steric constraints that control both the distance and orientation of the probes in the peptides examined, that vary depending on the number of Aib residues in the spacer. Briefly, we started by putting the backbone chain of $P(Aib)_nN$ in a 3_{10}-helix, in agreement with both IR and ^1H NMR results. We then built up for each peptide the conformers arising from the internal rotation of all angles of the probes linkages, making use of the rotational isomeric state model.[30] The total potential energy was evaluated in terms of electrostatic (COUL), nonbonding (NB) and hydrogen bond (HB) interactions, while 3-fold torsional potential functions (TOR), with barriers $V_0 = 1.2$ and 2.8 kcal/mol, were adopted for rotation around the N−C and C−C bonds. Standard bond angles and bond lengths were used for both backbone and side chains.[31] Nonbonded interatomic interactions were evaluated by using a 6−12 LJ potential function,[32−34a] hydrogen bond interactions were modeled by a dipole−dipole function, i.e., D/r^3, where $D = -230.1$ kJ·mol^{-1}·Å^3,[32b] and Coulombic interactions were assessed by assigning partial atomic charges for each atom in the peptides and a distance-dependent dielectric constant.[32b,c] Eventually, energy minimization refinement was performed by relaxing the fixed geometry for all the internal degrees of freedom, including those of the ordered backbone chain.[9,11,34b,c] For this purpose, eq 2 was used, comprising stretching and bending terms (STR and BEN),[35] besides the aforementioned potential functions.

$$U_m = \mathrm{COUL} + \mathrm{HB} + \mathrm{NB} + \mathrm{TOR} + \mathrm{STR} + \mathrm{BEN} \quad (2)$$

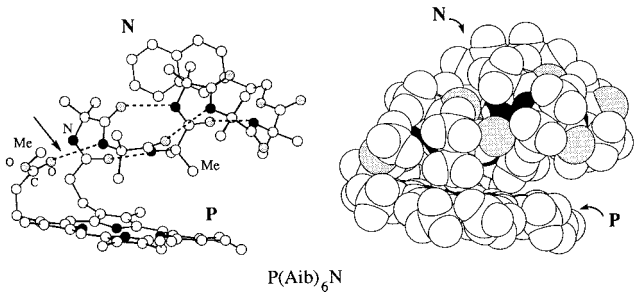

Figure 7. Theoretical model of the deepest energy minimum conformer of $P(Aib)_6N$ in methanol, with the backbone chain in the right-handed 3_{10}-helix, viewed end to the helix axis. Broken lines represent the intramolecular H-bonds, while the arrow indicates the additional H-bond as compared to the corresponding Z-analogue. Nitrogen atoms are in black, oxygen atoms are dotted, and hydrogen atoms are omitted for clarity. The space-filling model is also reported, showing how good are the contacts between the probes and the backbone chain, giving rise to a highly compact structure.

Table 5. Molecular Parameters of the Deepest Energy Minima Conformers and of the Next Most Favored Conformers of $P(Aib)_nN$ in Methanol

peptides	ΔU_m[a] (kcal/mol)	R_m[b] (Å)	$10^2\kappa_m{}^2$[c]
$P(Aib)_3N$	0	10.73	1.78
	2.69	10.30	0.03
$P(Aib)_6N$	0	11.60	1.41
	2.73	10.77	0.07
$P(Aib)_9N$	0	17.71	3.68
	0.85	15.84	0.75
$P(Aib)_{12}N$	0	19.86	2.29
	0.80	20.22	7.26
$P(Aib)_{15}N$	0	20.23	1.27
	0.29	26.40	2.38

[a] $\Delta U_m = U_m - U_{m,\min}$, where ΔU_m is the difference between the total energy of the mth conformer, eq 2, and the lowest energy among all conformers of the given peptide, $U_{m,\min}$. [b] P−N center-to-center distance. [c] Orientation parameter between P and N, from eq 5.

As a general observation, it appears that the peptides investigated exhibit a rigid structure, owing to both the 3_{10}-helix conformation of the backbone and the very short (2−3 σ bonds only) linkages of the probes. As a result, for each peptide only one or two, highly compact, conformers populate the solution, the loss in molecular entropy being overbalanced by energetic effects, owing to the multicenter attractive interactions, as shown, e.g., by the space-filling model of the deepest energy minimum conformer of $P(Aib)_6N$, reported in Figure 7. Other computed conformations have definitely higher energies (>2 kcal/mol), being thus negligible. The molecular parameters of the deepest energy minimum conformations are reported in Table 5, together with those of the next most favored conformers. Incidentally, because of the plane of pseudo-simmetry of protoporphyrin, the 2- and 18-monoester positional isomers of the peptides investigated are characterized by a very similar overall structure, exhibiting quite the same interprobe distances and mutual orientations and total energy, as well, according to computational data. Therefore, they are indistinguishable in terms of time decay results and related parameters.

We then addressed the problem of a quantitative comparison between the experimental data and computed structures, by taking into account both the quenching efficiencies and relative populations of the peptides investigated.

The quenching efficiency from time-resolved experiments is given by

$$E_i = 1 - (\tau_{Ni}/\tau_{N0}) \quad (3)$$

while that calculated according to the dipole−dipole interaction model[27] is given by eq 4.

$$E_m = \{1+[2/(3\kappa_m{}^2)](R_m/R_0)^6\}^{-1} \quad (4)$$

Here R_m is the center-to-center distance of the probes in the mth conformer, and $\kappa_m{}^2$ a dimensionless geometric factor determined by the orientation in space of the transition dipole moments of the donor and acceptor, i.e.,[27,36]

$$\kappa_m{}^2 = \cos^2\theta\,(3\cos^2\gamma + 1) \quad (5)$$

Provided that the donor and acceptor molecules do not rotate fast enough to randomize their orientation during the donor lifetime, a particular relative orientation between the probes is described by two angles only, γ and θ, where $0 \le \gamma$ and $\theta \le \pi$. The scheme used to evaluate the orientations in space of the transition dipole moments of N* and P was already illustrated.[10b,34b,c] In contrast, when rapid relative rotations occur, the "dynamic" isotropic average of the orientation factor, $\langle\kappa^2\rangle = {}^2/_3$, is used.[37] Finally, R_0 is the distance at which 50% transfer of excitation energy occurs, namely:[2]

$$R_0 = 9.79 \times 10^3[({}^2/_3\Phi_N J_F)/n^4]^{1/6} \quad (6)$$

where Φ_N is the quantum yield of N, n the refractive index of the solvent, and J_F ($M^{-1}\cdot cm^3$) the overlap integral calculated from the donor fluorescence and acceptor absorption spectra. From the spectral patterns of the normalized donor fluorescence and the acceptor extinction coefficient, already reported,[34a] the overlap integral in methanol is 1.30×10^{-13} $M^{-1}\cdot cm^3$, and hence R_0 is 42.2 Å.

The preexponents of the fluorescence decay, measuring the relative populations of each conformer with a given quenching efficiency, and the Boltzmann weight for that conformer, as given by eq 7 (where the sum is over all conformers), are listed in Table 6, together with the experimental and calculated quenching efficiencies.

$$P_m = \exp(-U_m/RT)/\sum_m \exp(-\Delta U_m/RT) \quad (7)$$

The main inferences to be drawn from Table 6 are 5-fold. First, by using the interprobe distance and orientation parameter of the low-energy conformers (Table 5) to estimate Förster energy transfer efficiencies, $E_{m,calcd}$ (eq 4), the agreement between these values and those experimentally observed, $E_{i,exp}$ (eq 3, where i goes from 1 to 3), is very good, except for P(Aib)$_{15}$N. Note that $E_{m,calcd}$ refers to the most favored computed structures, i.e., $m = 1$ for the first two peptides and $m = 1$ and 2 for the remaining three peptides. Second, where the relative energies of the sterically most favored structures were employed to estimate the Boltzmann probability of each conformer, the agreement between P_m and the lifetimes preexponent, α_{Ni}, is satisfactory

Table 6. Comparison between Experimental and Calculated Quenching Efficiency and Relative Population of the Most Favored Conformers in Methanol Solution

P(Aib)$_n$N	$E_{i,exp}$[a]	$E_{m,calcd}$[b]	α_{Ni}[c]	P_m[d]
P(Aib)$_3$N	0.99	0.99	0.93	0.92
	0.69		0.03	
	0.07		0.04	
P(Aib)$_6$N	0.97	0.98	0.96	0.97
	0.79		0.03	
	0.08		0.01	
P(Aib)$_9$N	0.92	0.91, 0.80	0.73	0.79, 0.19
	0.83		0.23	
	0.07		0.04	
P(Aib)$_{12}$N	0.89	0.90, 0.76	0.26	0.20, 0.77
	0.74		0.71	
	0.17		0.03	
P(Aib)$_{15}$N	0.92	0.61, 0.37	0.09	0.60, 0.37
	0.65		0.60	
	0.17		0.31	

[a] From eq 3. [b] From eq 4. [c] Lifetime preexponents, from Table 3, to be compared with the values of P_m. [d] From eq 7, the uncertainty being within ±0.01.

in all cases. In this connection, it is worth noting that P_m has exactly the same meaning as α_{Ni}, provided that static quenching is absent,[38] as it is here the case (see above). Third, both these results take partially into account the role played by the solvent medium in controlling the features of the computed conformations, since the Coulombic term in eq 2 includes the dielectric constant of the solvent (methanol). $E_{m,calcd}$ is also solvent-dependent, being estimated from R_0, which depends on the solvent through the values of J_F, Φ_N, and n, eq 6. Fourth, the length of the ordered backbone chain controls the spatial disposition of the chromophores, and hence the overall topology of the peptides, in the sense that the longer the chain the higher the probability that the P and N molecules are accommodated on the same side of the surface of the helix. This is illustrated in Figure 8, where the deepest energy minimum conformers of P(Aib)$_{15}$N are reported. Interestingly enough, there is an additional intramolecular H-bond in all peptides investigated (see also Figure 7), as compared to those present in the ordered backbone chain of the corresponding Z−(Aib)$_n$N analogues, which further stiffens the overall structure, and is responsible for the higher A_b/A_f ratios shown in Figure 1.[23] It involves the peptide N(2)−H group and the CO group of the methyl ester moiety of P. Fifth, theoretical quantities were found to well reproduce the experimental ones only when the mutual orientation of the probes were taken into account in interpreting the fluorescence decay results, which implies that interconversion among conformational substates of N linkages is slow on the time scale of the energy transfer process for all peptides examined.[36]

Overall, these findings give great confidence in the energetically most favored computed structures, and make it reasonable to consider them as a good representation of the conformations populating the methanol solution.

Electron Transfer vs Energy Transfer Quenching Mechanism. The disagreement between experimental and calculated transfer efficiencies for P(Aib)$_{15}$N (Table 6), and the peculiar fluorescence behavior of this peptide, as compared to the other ones (e.g., Table 1), may be explained by taking into account the occurrence of a competitive mechanism of N* quenching, not involving the P excited states. A P → N* electron-

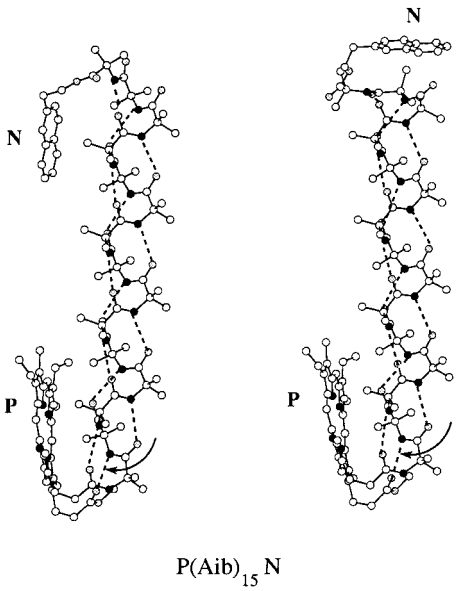

Figure 8. Theoretical models of the deepest energy minimum conformers of P(Aib)$_{15}$N in methanol, with the backbone chain in the right-handed 3_{10}-helix, viewed perpendicularly to the helix axis. Broken lines represent the intramolecular H-bonds, while the arrows indicate the additional H-bond in each conformer as compared to the corresponding Z-analogue. Nitrogen atoms are in black, oxygen atoms are dotted, and hydrogen atoms are omitted for clarity. Note the edge-to-edge arrangement of the probes lying on the surface of the helix in one conformer (left), which may favor a P → ^{1}N* electron transfer, competing with the energy transfer.

transfer process was thus thought to take place,[8] in agreement with the results of flash photolysis (Figure 6a). Therefore, a competition between energy and electron transfer is likely to occur in the high terms of the series, resulting from a complex interplay of electronic, Franck−Condon and topological factors. As the length of the ordered P(Aib)$_n$N increases, the probability that at least one conformer is characterized by a steric arrangement where the P and N molecules are lying on the same side of the surface of the helix increases (Figure 8).[39] This topology would be such as to control the nuclear mobility of the probes, and to enhance the d/a electronic coupling by optimizing the donor-to-bridge and bridge-to-acceptor orbital matching.[4,5]

Several interacting electron-transfer proteins and polypeptides exhibit a heme-edge-to-heme-edge geometry,[40,41] while the influence of the helical structure of peptidic bridges on ET is well documented.[6,42] Both the electric field originated by the macroscopic dipole moment of the helix[42] and the good matching of the d/a orbitals with that of the bridge, as compared to random coil,[6] can facilitate ET. Indeed, comparison among rigid spacers has shown that electronic transmission across peptides is more facile than, e.g., across saturated hydrocarbons.[43] Therefore, the switch in the overall topology of the peptides investigated, from a twisted geometry of the probes in the short terms of the series (Figure 7) to an edge-to-edge geometry, where both the rings of the N and P probes are parallel to the helical axis, in the longest term of the series (Figure 8), very likely determines the shift from energy transfer to electron-transfer quenching of N*. This for, at least, two reasons. First, because it shortens the d/a distance by about 6 Å, as compared to the other isomer of P(Aib)$_{15}$N (Table 5), where the probes do not lie on the surface of the helix, and second, because it fixes the d/a pair in place along the helix, modulating the electronic coupling pathway.

Concluding Remarks

From the data set considered here, three major conclusions can be drawn. First, P(Aib)$_n$N peptides in methanol experience electronic energy transfer from excited naphthalene to ground-state porphyrin as the major excited-state process in the nanosecond domain. Second, orientational effects between the probes must be taken into account for a correct interpretation of fluorescence decay data, which implies that interconversion among conformational substates of N linkages is slow on the time scale of the transfer process; i.e., it is slower than 10 ns. This is fully consistent with computational results showing that the sterically most favored conformers populating the methanol solution are characterized by highly compact structures. Third, as the length of the backbone chain increases, a competitive mechanism of N* quenching takes place, possibly a P → N* ET process. The topology of the high terms of the series, chiefly P(Aib)$_{15}$N, seeing the P and N molecules accommodated on the surface of the 3_{10}-helix in an edge-to-edge arrangement, apparently improves the electronic coupling of the interacting P and N* molecules, thus playing a critical role in facilitating an ET process.

Acknowledgment. This work was supported in part by MURST and in part by the Italian National Research Council (CNR).

References and Notes

(1) See, for example: (a) Kavarnos, G. J.; Turro, N. J. *Chem. Rev.* **1986**, *86*, 401. (b) Wasielewski, M. R. *Chem. Rev.* **1992**, *92*, 435, and references therein.

(2) Förster, T. *Ann. Phys. (Leipzig)* **1948**, *2*, 55; *Discuss. Faraday Soc.* **1959**, *27*, 7.

(3) Hirata, Y.; Kanda, Y.; Mataga, N. *J. Phys. Chem.* **1983**, *87*, 1659.

(4) (a) Marcus, R. A.; Sutin, N. *Biochim. Biophys. Acta* **1985**, *811*, 265. (b) Sutin, N. In *Electron Transfer in Inorganic, Organic and Biological Systems*, Bolton, J. R., Mataga, N., McLendon, G., Eds.; Advances in Chemistry Series 228; American Chemical Society: Washington, DC, 1991; p 25. (c) Newton, M. D. *Chem. Rev.* **1991**, *91*, 767. (d) Evenson, J. W.; Karplus, M. *Science* **1993**, *262*, 1247.

(5) See, for example: (a) *Electron and Proton Transfer. J. Chem. Soc., Faraday Discuss.* **1982**, *74*. (b) Ungar, L. W.; Newton, M. D.; Voth, G. A. *J. Phys. Chem. B* **1999**, *103*, 7367. (c) Beratan, D. N.; Onuchic, J. N. In *Protein Electron Transfer*; Bendall, D. S., Ed.; Bios Scientific Publishers: Oxford, U.K., 1996; Chapter 2.

(6) (a) Isied, S. S. In *Electron Transfer in Inorganic, Organic and Biological Systems*; Bolton, J. R., Mataga, N., McLendon, G., Eds.; Advances in Chemistry Series 228; American Chemical Society: Washington, DC, 1991; p 229. (b) Vassilian, A.; Wishart, J.; van Hemelryck, B.; Schwartz, H.; Isied, S. S. *J. Am. Chem. Soc.* **1990**, *112*, 7278.

(7) (a) Bolton, J. R. In *Electron Transfer in Inorganic, Organic and Biological Systems*, Bolton, J. R., Mataga, N., McLendon, G., Eds.; Advances in Chemistry Series 228; American Chemical Society: Washington, DC, 1991; p 117. (b) Schmidt, J. A.; Siemiarczuk, A.; Weedon, A. C.; Bolton, J. R. *J. Am. Chem. Soc.* **1985**, *107*, 6112.

(8) Pispisa, B.; Venanzi, M.; Palleschi, A. *J. Chem. Soc., Faraday Trans.* **1994**, *90*, 1857. Pispisa, B.; Venanzi, M.; D'Alagni, M. *Biopolymers* **1994**, *34*, 435. Pispisa, B.; Venanzi, M.; Palleschi, A.; D'Alagni, M. *Macromol. Chem. Phys.* **1995**, *196*, 2809.

(9) (a) Pispisa, B.; Venanzi, M.; Palleschi, A.; Zanotti, G. *J. Photochem. Photobiol., A: Chem.* **1997**,*105*, 225. (b) Pispisa, B.; Palleschi, A.; Venanzi, M.; Zanotti, G.; Stella, L. *Res. Dev. Photochem. Photobiol.*, **1999**, *3*, 11.

(10) (a) Pispisa, B.; Venanzi, M.; Palleschi, A.; Zanotti, G. *J. Mol. Liq.* **1994**, *61*, 167. (b) Pispisa, B.; Venanzi, M.; Palleschi, A.; Zanotti, G. *Macromolecules* **1994**, *27*, 7800.
(11) Pispisa, B.; Venanzi, M.; Palleschi, A.; Zanotti, G. *Biopolymers* **1995**, *36*, 497.
(12) (a) Karle, I. L.; Balaram, P. *Biochemistry* **1990**, *29*, 6747. (b) Toniolo, C.; Benedetti, E. *Macromolecules* **1991**, *24*, 4004. (c) Toniolo, C.; Benedetti, E. *Trends Biochem. Sci.* **1991**, *16*, 350.
(13) Früchtel, J. S.; Jung, G. *Angew. Chem., Int. Ed. Engl.* **1996**, *35*, 17.
(14) Jones, D. S.; Kenner, G. W.; Preston, J.; Sheppard, R. C. *J. Chem. Soc.* **1965**, 6227.
(15) (a) Chen, F. M. F.; Kuroda, K.; Benoiton, N. L. *Synthesis* **1978**, 928. (b) McGahren, W. J.; Goodman, M. *Tetrahedron* **1967**, *23*, 2017. (c) Valle, G.; Formaggio, F.; Crisma, M.; Bonora, G. M.; Toniolo, C.; Bavoso, A.; Benedetti, E.; Di Blasio, B.; Pavone, V.; Pedone, C. *J. Chem. Soc., Perkin Trans. 2* **1986**, 1371.
(16) Leplawy, M. T.; Jones, D. S.; Kenner, G. W.; Sheppard, R. C. *Tetrahedron* **1960**, *11*, 39.
(17) Carpino, L. A. *J. Am. Chem. Soc.* **1993**, *115*, 4397.
(18) (a) Wang, S. S. *J. Am. Chem. Soc.* **1973**, *95*, 1328. (b) Lu, G.; Mojsov, S.; Tam, J. P.; Merrifield, R. B. *J. Org. Chem.* **1981**, *46*, 3433.
(19) Toniolo, C.; Bonora, G. M.; Crisma, M.; Benedetti, E.; Bavoso, A.; Di Blasio, B.; Pavone, V.; Pedone, C. *Int. J. Pept. Protein Res.* **1983**, *22*, 603.
(20) Eaton, D. F. *Pure Appl. Chem.* **1988**, *60*, 1107.
(21) (a) Mizushima, S.; Shimanouchi, T.; Tsuboi, M.; Souda, R. *J. Am. Chem. Soc.* **1952**, *74*, 270.(b) Palumbo, M.; Da Rin, S.; Bonora, G. M.; Toniolo, C. *Makromol. Chem.* **1976**, *177*, 1477. (c) Kennedy, D. F.; Crisma, M.; Toniolo, C.; Chapman, D. *Biochemistry* **1991**, *30*, 6541.
(22) IR measurements at variable concentrations demonstrated that, even at 10 mM concentration, self-association via intermolecular H-bonding was negligible for all peptides.
(23) The experimental parameter A_b/A_f is given by: $A_b/A_f = (n_b/n_f)(\epsilon_b/\epsilon_f)$, where $n_{b(f)}$ is the number of H-bonded (free) N−H groups and $\epsilon_{b(f)}$ the corresponding molar extinction coefficient. Since P(Aib)$_n$N experience an additional intramolecular H-bond as compared to Z−(Aib)$_n$N (see Figures 7 and 8), comparison of this parameter for the two series of peptides requires an adjustment for P(Aib)$_n$N; i.e., the A_b/A_f ratio must be multiplied by $(n_f/n_b)[(n_b - 1)/(n_f + 1)]$.
(24) Kopple, K. D.; Ohnishi, M. *Biochemistry* **1969**, *8*, 4087.
(25) Toniolo, C.; Bonora, G. M.; Barone, V.; Bavoso, A.; Benedetti, E.; Di Blasio, B.; Grimaldi, P.; Lelj, M.; Pavone, V.; Pedone, C. *Macromolecules* **1985**, *18*, 895.
(26) Mataga, N. In *Electron Transfer in Inorganic, Organic and Biological Systems*, Bolton, J. R.; Mataga, N., McLendon, G., Eds.; Advances in Chemistry Series 228; American Chemical Society: Washington, DC, 1991; p 91.
(27) (a) Steinberg, I. Z. *J. Chem. Phys.* **1968**, *48*, 2411. (b) Grinvald, A.; Haas, E.; Steinberg, I. Z. *Proc. Natl. Acad. Sci., U.S.A.* **1972**, *69*, 2273.
(28) (a) Sinclair, R. S.; Tait, D.; Truscott, T. G. *J. Chem. Soc., Faraday Trans. 1* **1980**, *76*, 417. (b) Nahor, G. S.; Rabani, J.; Grieser, F. *J. Phys. Chem.* **1981**, *85*, 697.
(29) (a) McIntosh, A. R.; Siemiarczuk, A.; Bolton, J. R.; Stillman, M. J.; Ho, T.-F.; Weedon, A. C. *J. Am. Chem. Soc.* **1983**, *105*, 7215. (b) Wasielewski, M. R.; Niemczyk, M. P. *J. Am. Chem. Soc.* **1984**, *106*, 5043. (c) Manna, B. Kr.; Sen, D.; Bera, S. Ch.; Rohatgi-Mukherjee K. K. *Chem. Phys. Lett.* **1991**, *176*, 191.
(30) Mattice, W. L.; Suter, U. W.*Conformational Theory of Large Molecules*; Wiley: New York, 1994.
(31) Wunderlich, H.; Mootz, D. *Acta Crystallogr., Sect B* **1971**, *27*, 1684. Andersen, A. M. *Acta Chem. Scand., Ser. B* **1975**, *29*, 239.
(32) (a) Pispisa, B.; Palleschi, A.; Barteri, M.; Nardini, S. *J. Phys. Chem.* **1985**, *89*, 1767. (b) Pispisa, B.; Palleschi, A. *Macromolecules* **1986**, *19*, 904. (c) Pispisa, B.; Palleschi, A.; Paradossi, G. *J. Phys. Chem.* **1987**, *91*, 1546. Pispisa, B.; Paradossi, G.; Palleschi, A.; Desideri, A. *J. Phys. Chem.* **1988**, *92*, 3422.
(33) Nemethy, G.; Pottle, M. S.; Scheraga, H. A. *J. Phys. Chem.* **1983**, *87*, 1883.
(34) (a) Pispisa, B.; Palleschi, A.; Venanzi, M.; Zanotti, G. *J. Phys. Chem. B* **1996**, *100*, 6835, and references therein. (b) Pispisa, B.; Palleschi, A.; Amato, M. E.; Segre, A. L.; Venanzi, M. *Macromolecules* **1997**, *30*, 4905. (c) Pispisa, B.; Venanzi, M.; Stella, L.; Palleschi, A.; Zanotti, G. *J. Phys. Chem. B* **1999**, *103*, 8172,
(35) Allinger, N. L. *J. Am. Chem. Soc.* **1997**, *119*, 8127. Burkert, J.; Allinger, N. L. *Molecular Mechanics*; American Chemical Society: Washington, DC, 1982.
(36) van der Meer, B. W. In *Resonance Energy Transfer*, Andrews, D. L., Demidov, A. A., Eds; Wiley: New York, 1999; Chapter 4.
(37) (a) Bednár, B.; Morawetz, H.; Shafer, J. A. *Macromolecules* **1985**, *18*, 1940. (b) McWherter, C. A.; Haas, E.; Leed, A. R.; Scheraga, H. A. *Biochemistry* **1986**, *25*, 1951. (c) Kaschke, M.; Ernsting, N. P.; Valeur, B.; Bourson, J. *J. Phys. Chem.* **1990**, *94*, 5757. (d) Liu, G. *Macromolecules* **1993**, *26*, 1144.
(38) Pispisa, B.; Palleschi, A.; Stella, L.; Venanzi, M.; Toniolo, C. *J. Phys. Chem. B* **1998**, *102*, 7890.
(39) Solubility problems prevented, unfortunately, the synthesis of further terms of the series, e.g., P(Aib)$_{18}$N, which would have made it possible to draw a definite conclusion on this issue.
(40) (a) Salemme, F. R. In *Tunneling in Biological Systems*, Chance, B., DeVault, D. C., Frauenfelder, H., Marcus, R. A., Schrieffer, J. R., Sutin, N., Eds.; Academic Press: New York, 1979; p 523. (b) Dixon, D. W.; Hong, X.; Woehler, S. E.; Mauk, A. G.; Sishta, B. P. *J. Am. Chem. Soc.* **1990**, *112*, 1082.
(41) Inai, Y.; Sisido, M.; Imanishi, Y. *J. Phys. Chem.* **1990**, *94*, 6237.
(42) Fox, M. A.; Galoppini, E. *J. Am. Chem. Soc.* **1997**, *119*, 5277.
(43) Closs, G. L.; Miller, J. R. *Science* **1988**, *240*, 440.

MA991539O